

KAN-AE with Non-Linearity Score and Symbolic Regression for Energy-Efficient Channel Coding

Anthony Joseph Perre, Parker Huggins, and Alphan Sahan

Department of Electrical Engineering, University of South Carolina, Columbia, SC, USA

Email: {aperre, parkerkh}@email.sc.edu, asahin@mailbox.sc.edu

Abstract—In this paper, we investigate Kolmogorov-Arnold network-based autoencoders (KAN-AEs) with symbolic regression (SR) for energy-efficient channel coding. By using SR, we convert KAN-AEs into symbolic expressions, which enables low-complexity implementation and improved energy efficiency at the radios. To further enhance the efficiency, we introduce a new non-linearity score term in the SR process to help select lower-complexity equations when possible. Through numerical simulations, we demonstrate that KAN-AEs achieve competitive BLER performance while improving energy efficiency when paired with SR. We score the energy efficiency of a KAN-AE implementation using the proposed non-linearity metric and compare it to a multi-layer perceptron-based autoencoder (MLP-AE). Our experiment shows that the KAN-AE paired with SR uses 1.38 times less energy than the MLP-AE, supporting that KAN-AEs are a promising choice for energy-efficient deep learning-based channel coding.

Index Terms—autoencoder, channel coding, energy efficiency, Kolmogorov-Arnold network

I. Introduction

Deep learning (DL) has been demonstrated to enhance traditional signal processing techniques in modern wireless communication systems. For example, DL approaches are used to improve channel estimation and recognize modulation type in [1] and [2], respectively. Furthermore, DL has been applied to learn joint source and channel coding tasks within end-to-end orthogonal frequency-division multiplexing (OFDM) systems [1, 2]. Although the application of DL models to wireless communications shows great promise, their adoption in practical systems faces several challenges. One of the main issues lies in mobile device hardware, where constrained memory resources and CPU capabilities limit the efficacy of large DL models at the radios [3]. Complex models with hundreds of thousands of learnable parameters cause memory and timing issues for mobile devices, which in turn leads to increased energy and power consumption [4]. Hence, there is a clear need for more efficient model architectures that can reduce memory usage and computational load without having to sacrifice performance.

Multi-layer perceptrons (MLPs) are a fundamental component of various DL architectures. Recently, a novel DL structure called Kolmogorov-Arnold networks (KANs)

have emerged as an alternative to MLPs [5]. Studies show that KANs outperform MLPs in accuracy while requiring fewer total parameters [5]. The authors of [6] challenge some of the claims made in [5], but confirm that KANs outperform MLPs in symbolic formula representation under fair comparison. Recently, KANs have seen extensive use in various domains such as physics and time series prediction, particularly for their increased interpretability and symbolic representation capabilities [7, 8]. Of particular interest to this work is the reduced number of parameters required by KANs, which makes them more suitable for resource-constrained environments like mobile devices, where memory and computational resources are limited. Additionally, KANs are highly compatible with SR, which means that the learned network can be expressed as a combination of simpler symbolic equations. These expressions can improve energy efficiency by reducing the complexity and resource demands of executing the model.

In this study, we investigate the use of autoencoders (AEs) for channel coding, which is discussed in several prior works [9, 10, 11]. In our approach, we replace MLPs in the AE structure with KANs, which we find to demonstrate comparable block error rate (BLER) performance while having fewer total parameters. Once the entire KAN-AE is trained, we use SR to derive equations representing the learned behavior. Furthermore, we introduce a non-linearity score term into the SR process to encourage simpler equations when feasible. Our use of SR, combined with the proposed non-linearity score term, aims to lower the energy consumption of the AE model. By using KANs, we show that it is possible to reduce the energy usage of certain DL architectures without sacrificing performance, which suggests that KANs can be a useful alternative to MLPs for specific DL tasks within wireless communications.

Organization: The paper is organized as follows. Section II presents the system model and provides fundamental concepts related to KANs. Section III describes the proposed KAN-AE and the metrics used to assess energy efficiency. Section IV shows the BLER performance and compares the energy efficiency of each model. Section V concludes the paper.

Notation: The set of real and complex numbers are

This work has been supported by the National Science Foundation (NSF) through the award CNS-2438837.

denoted by \mathbb{R} and \mathbb{C} , respectively. The complex conjugate of $z = a + jb$ is expressed as $z^* = a - jb$. The circularly symmetric complex normal distribution with zero mean and variance σ^2 is represented as $\mathcal{CN}(0, \sigma^2)$. The Hermitian of a matrix \mathbf{A} is denoted by \mathbf{A}^H . $\mathbb{E}[X]$ denotes the expected value of X .

II. System Model

In this section, we discuss preliminaries on KANs and provide our system model on OFDM-based AEs.

A. Kolmogorov-Arnold Networks

The structure of KANs is inspired by the Kolmogorov-Arnold representation theorem, which establishes that any multi-variate continuous function can be expressed as the sum of several uni-variate continuous functions [12], i.e.,

$$f(x_1, x_2, \dots, x_d) = \sum_{i=0}^{2d} \Phi_i \left(\sum_{j=1}^d \phi_{i,j}(x_j) \right), \quad (1)$$

where $\phi_{i,j} : [0, 1] \rightarrow \mathbb{R}$ and $\Phi_i : \mathbb{R} \rightarrow \mathbb{R}$. The authors of [5] generalize the inner and outer sums in (1) to accommodate an arbitrary number of layers L as

$$\begin{aligned} \text{KAN}(\mathbf{x}) &= (\Phi^{(L)} \circ \Phi^{(L-1)} \circ \dots \circ \Phi^{(2)} \circ \Phi^{(1)})(\mathbf{x}) \quad (2) \\ &= \sum_{i_{L-1}=1}^{d_{L-1}} \phi_{i_L, i_{L-1}}^{(L)} \left(\dots \sum_{i_1=1}^{d_1} \phi_{i_2, i_1}^{(2)} \left(\sum_{i_0=1}^{d_0} \phi_{i_1, i_0}^{(1)}(x_{i_0}) \right) \dots \right), \end{aligned}$$

where $\phi_{i_l, i_{l-1}}^{(l)}(\cdot)$ is a learnable function in the l th layer connecting the i_{l-1} th input neuron to the i_l th output neuron, i.e., an edge, d_l is the number of neurons in the l th layer, $\Phi^{(l)}$ contains all learnable activation functions at the l th layer as

$$\Phi^{(l)}(\cdot) \triangleq \begin{bmatrix} \phi_{1,1}^{(l)}(\cdot) & \dots & \phi_{1,d_{l-1}}^{(l)}(\cdot) \\ \vdots & \ddots & \vdots \\ \phi_{d_l,1}^{(l)}(\cdot) & \dots & \phi_{d_l,d_{l-1}}^{(l)}(\cdot) \end{bmatrix}, \quad (3)$$

and operates on the output of the previous layer $\mathbf{a}^{(l-1)} \in \mathbb{R}^{d_{l-1}}$, for $\forall l \in \{1, \dots, L\}$, as

$$\mathbf{a}^{(l)} = \Phi^{(l)}(\mathbf{a}^{(l-1)}) \triangleq \begin{bmatrix} \sum_{i_{l-1}=1}^{d_{l-1}} \phi_{i_l, i_{l-1}}^{(l)}(a_{i_{l-1}}^{(l-1)}) \\ \vdots \\ \sum_{i_{l-1}=1}^{d_{l-1}} \phi_{i_l, i_{l-1}}^{(l)}(a_{i_{l-1}}^{(l-1)}) \end{bmatrix}.$$

Here, an edge refers to a connection between an input and an output neuron that performs some transformation on the input. While the weights on the edges are learnable and the activation functions are fixed in MLPs, the opposite holds for KANs.

In [5], the authors express an activation function $\phi(x)$ as a linear combination of B-splines and sigmoid linear

unit (SiLU), i.e.,

$$\phi(x) = w_b \times \text{SiLU}(x) + w_s \times \sum_i (c_i \times B_i(x)), \quad (4)$$

where $B_i(x)$ is a B-spline basis function, composed of piecewise polynomials of degree p and scaled by a learnable weight c_i . The parameters w_b and w_s are also learnable. Each B-spline is defined on a specific grid interval, which is determined by the range of input samples.

B. System Model

Consider a single-user communication link. Let $r = k/n$ be the rate of this communication link, where k is the total number of information bits per message and n is the total number of channel uses. Let $\mathbf{s}_m \in \mathbb{R}^{2^k}$ be a one-hot encoded (OHE) vector representation of the message m . The encoder network $\epsilon(\mathbf{s}_m)$ maps \mathbf{s}_m to the vector $\mathbf{s}_e \in \mathbb{R}^n$, which is then converted to the real and imaginary components of $s_{tx} \in \mathbb{C}^{n/2}$, where $\mathbb{E}[|s_{tx}|^2] = 1$. We consider L_{enc} layers at the encoder. For an MLP-based neural network, we have

$$\mathbf{a}_{\text{enc}}^{(l)} = \sigma_{\text{enc}}^{(l)}(\mathbf{W}_{\text{enc}}^{(l)} \mathbf{a}_{\text{enc}}^{(l-1)} + \mathbf{b}_{\text{enc}}^{(l)}), \quad l = 1, \dots, L_{\text{enc}}, \quad (5)$$

where $\sigma_{\text{enc}}^{(l)}$ is the element-wise non-linear activation function, and $\mathbf{W}_{\text{enc}}^{(l)} \in \mathbb{R}^{d_l \times d_{l-1}}$ and $\mathbf{b}_{\text{enc}}^{(l)} \in \mathbb{R}^{d_l}$ are the weight matrix and bias vector, respectively. We note that for both the MLP and KAN models, $\mathbf{a}_{\text{enc}}^{(0)} = \mathbf{s}_m$ and $\mathbf{a}_{\text{enc}}^{(L_{\text{enc}})} = \mathbf{s}_e$. However, for a KAN-based neural network, by re-expressing (2), we have

$$\mathbf{a}_{\text{enc}}^{(l)} = \Phi_{\text{enc}}^{(l)}(\mathbf{a}_{\text{enc}}^{(l-1)}), \quad l = 1, \dots, L_{\text{enc}}, \quad (6)$$

where $\Phi_{\text{enc}}^{(l)}$ is $d_l \times d_{l-1}$ function space and $\mathbf{a}_{\text{enc}}^{(0)} = \mathbf{s}_m$. In this study, we use (4) to learn the activation functions in KANs.

After encoding at the transmitter, the transmitted symbols s_{tx} propagate through a communication channel, where they are distorted by the channel and by zero-mean, circularly symmetric complex additive white Gaussian noise (AWGN). Let h denote the channel coefficient. A received symbol s_{rx} can then be expressed as

$$s_{rx} = hs_{tx} + w, \quad (7)$$

for $w \sim \mathcal{CN}(0, \sigma_n^2)$. Under an AWGN channel, we set $h = 1$. For a flat-fading Rayleigh channel, such as that observed by an OFDM subcarrier, we instead model $h \sim \mathcal{CN}(0, 1)$ and assume that h is known at the receiver. Then, s_{rx} are equalized using a minimum mean-squared error (MMSE) equalizer, which yields $\hat{s}_{rx} = \frac{h^* s_{rx}}{|h|^2 + \sigma_n^2}$, where \hat{s}_{rx} is the estimated transmitted symbol after equalization. The real and imaginary components of $\hat{s}_{rx} \in \mathbb{C}^{n/2}$ are then converted to a single real-valued vector $\mathbf{s}_d \in \mathbb{R}^n$.

Let $\delta(\mathbf{s}_d)$ denote the decoder network that maps \mathbf{s}_d to a vector $\hat{\mathbf{s}}_m \in \mathbb{R}^{2^k}$ of logarithmic odds. For L_{dec} layers, the MLP-based and KAN-based decoders follow the structures

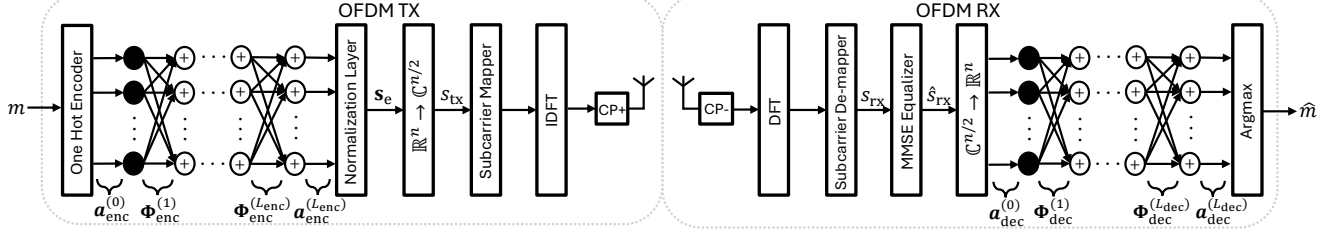


Fig. 1. OFDM transmitter and receiver block diagrams with an (n, k) KAN-AE.

in (5) and (6), respectively. Furthermore, we define $\mathbf{a}_{\text{dec}}^{(0)} = \mathbf{s}_d$ and $\mathbf{a}_{\text{dec}}^{(L_{\text{dec}})} = \hat{\mathbf{s}}_m$. The detected message \hat{m} is expressed as

$$\hat{m} = \arg \max_{\hat{\mathbf{s}}_m \in \mathbb{R}^{2^k}} \hat{\mathbf{s}}_m . \quad (8)$$

Conventional single-layer neural networks, also known as perceptrons, can only learn linear decision boundaries, which limits their ability to capture complex non-linear relationships. While MLPs address this limitation by stacking multiple layers, a single KAN layer is capable of modeling complex non-linear patterns due to the flexibility of its learnable activation functions. Fig. 1 illustrates a KAN-AE within an end-to-end OFDM transmitter and receiver, for a given n channel uses and k bits. Although we consider an arbitrary number of KAN layers at the transmitter and receiver, a single layer may be used in both cases.

III. Energy-Efficient KAN-based Autoencoder

In this work, we aim to reduce the number of learnable parameters in the encoder and decoder to improve energy efficiency at the transmitter and receiver, while maintaining a low BLER. We exploit that KANs are highly compatible with SR, and introduce a new penalty term in the SR process to discourage less energy-efficient symbolic expressions. The functions are heuristically scored by measuring non-linearity, as discussed in Section III-A and Section III-B. Our approach enables scoring the energy efficiencies of KAN and MLP networks regardless of the implementation, as discussed in Section III-C.

A. Quantifying Function Non-linearity

To quantify the degree of non-linearity for a function $f(x)$ over an interval $[a, b]$, we propose using a piecewise linear approximation. The idea is to assess the non-linearity of $f(x)$ based on the minimum number of linear segments, N , required to approximate $f(x)$ within a specified error tolerance, ϵ . The number of segments N then serves as a metric of non-linearity. A larger N indicates higher non-linearity, while a smaller N implies that $f(x)$ is closer to a linear form over $[a, b]$.

To express the aforementioned metric, consider a set of uniformly spaced partition points a_1, a_2, \dots, a_{N+1} for $a_1 = a$ and $a_{N+1} = b$, where $[a_j, a_{j+1}]$ is the j th sub-interval

on which $f(x)$ is linearly approximated. We express the approximation error over the j th sub-interval $[a_j, a_{j+1}]$ as

$$e_j = \int_{a_j}^{a_{j+1}} |f(x) - \psi_j(x)|^2 dx , \quad (9)$$

where $\psi_j(x) = m_j x + k_j$ is the best-fit linear approximation of $f(x)$ over $[a_j, a_{j+1}]$. To obtain $\psi_j(x)$, we oversample $f(x)$ in the j th subinterval and apply least squares regression, with m_j and k_j as the best-fit slope and intercept, respectively. We then measure the approximation error over all sub-intervals as

$$E(N) = \sum_{j=1}^N e_j . \quad (10)$$

The non-linearity measure of $f(x)$, denoted as $Q[f(x)]$, is the smallest N that satisfies $E(N) < \epsilon$, i.e.,

$$Q[f(x)] = \arg \min_N E(N) \quad \text{s.t.} \quad E(N) < \epsilon . \quad (11)$$

If $f(x)$ exhibits greater non-linearity, a larger N will be required to achieve the same approximation accuracy. Conversely, if $f(x)$ is more linear, a smaller N is required. The metric for $Q[f(x)]$ is formulated within the context of SR. Non-linear functions are often computationally intensive and energy demanding. Therefore, by determining $Q[f(x)]$, we can estimate the energy cost of approximating $f(x)$ and guide SR towards simpler approximations when feasible.

Example 1: Let $f(x) = |5x|$ and $g(x) = \sin(5x)$ be defined on the interval $[-1, 1]$ and assume an error tolerance $\epsilon = 10^{-3}$. For $f(x)$ and $g(x)$, compute $E(N)$ using (9) and (10). Repeat this process and increase N each iteration until the condition in (10) is satisfied. Then, (11) is used to determine the score for each function, yielding $Q[f(x)] = 2$ and $Q[g(x)] = 11$. This is expected, as $\sin(5x)$ is far more oscillatory on $[-1, 1]$ when compared to $|5x|$, thereby making it more non-linear.

B. Symbolic Regression under Non-linearity Constraint

Consider an activation function $\phi(x) \in [a, b] \rightarrow \mathbb{R}$ and a finite number of candidate functions $\{f_k(x)\}_{k=1}^K$ (e.g. sin, log, exp). Obtain samples $S(\phi) = \{\phi(x_i) \mid x_i \in [a, b]\}$. Let $\tilde{\phi}(x) = \gamma_0 f_k(\gamma_1 x + \beta_0) + \beta_0$ be an approximation of $\phi(x)$

Algorithm 1 Convert $\phi(x)$ to symbolic expression

Input: $S(\phi)$, $\{f_k(x)\}_{k=1}^K$
Output: $\phi_{\text{sym}}(x)$

$R_{\text{best}}^2 = -\infty$; $Z_{\text{best}} = -\infty$; $\hat{\phi}_k(x) = \text{None}$; $\phi_{\text{sym}}(x) = \text{None}$
 for $f_k(x)$ in $\{f_k(x)\}_{k=1}^K$ do
 $R_k^2 = -\infty$
 for (γ_i, β_i) in grid $[-10, 10]$ do
 Set $\tilde{\phi}(x) = \gamma_i f_k(\gamma_i x + \beta_i) + \beta_o$. Fit γ_o, β_o using
 linear regression with $S(\phi)$
 $R^2[\tilde{\phi}(x)] \leftarrow (12)$
 if $R^2[\tilde{\phi}(x)] > R_k^2$ then
 $\hat{\phi}_k(x) = \tilde{\phi}(x)$; $R_k^2 = R^2[\tilde{\phi}(x)]$
 end
 end
 $Z[\hat{\phi}_k(x)] \leftarrow (14)$
 if $Z[\hat{\phi}_k(x)] > Z_{\text{best}}$ then
 $\phi_{\text{sym}}(x) = \hat{\phi}_k(x)$; $Z_{\text{best}} = Z[\hat{\phi}_k(x)]$
 end
 end
 return $\phi_{\text{sym}}(x)$

given $\gamma_i, \beta_i, \gamma_o, \beta_o$, and $f_k(x)$. For each $\tilde{\phi}(x)$, we compute the R^2 score

$$R^2[\tilde{\phi}(x)] = 1 - \frac{\sum_{i=1}^N [\phi(x_i) - \tilde{\phi}(x_i)]^2}{\sum_{i=1}^N [\phi(x_i) - \bar{\phi}(x_i)]^2}, \quad (12)$$

where $\bar{\phi}(x_i) = \mathbb{E}[\phi(x_i)]$. Next, we set

$$\hat{\phi}_k(x) = \arg \max_{\phi(x)} R^2[\tilde{\phi}(x)], \quad (13)$$

where $\hat{\phi}_k(x)$ is the best approximation of $\phi(x)$ for a given $f_k(x)$. When determining the symbolic expression $\phi_{\text{sym}}(x)$ based on $\hat{\phi}_k(x)$, we utilize (11) and (12) to create a combined score term $Z[\hat{\phi}_k(x)]$, which is given by

$$Z[\hat{\phi}_k(x)] = R^2[\hat{\phi}_k(x)] + \frac{\lambda}{Q[\hat{\phi}_k(x)]}. \quad (14)$$

Here, λ weights the non-linearity score term. Using the combined score in (14), we compute

$$\phi_{\text{sym}}(x) = \arg \max_{\hat{\phi}_k(x)} Z[\hat{\phi}_k(x)]. \quad (15)$$

In this study, the parameters γ_i and β_i maximizing R^2 for a given $\phi(x)$ are determined using a grid search. Also, for each (γ_i, β_i) pair, γ_o and β_o are determined using least squares regression, where γ_o and β_o are the best-fit slope and intercept of $S(\phi)$, respectively. The described approach builds upon [5], with our proposed non-linearity score term added to encourage energy-efficient equations when possible. A thorough outline of the SR procedure is presented in Algorithm 1.

C. Scoring MLPs and KANs Based on Non-Linearity Metric

For a given MLP network, the total non-linearity score combines the individual scores for linear and non-linear activations. Thus, the total score $Q[\text{MLP}(\mathbf{x})]$ is expressed as

$$Q[\text{MLP}(\mathbf{x})] = \sum_{l=1}^L \left[d_l \times \left(d_{l-1} + Q[\sigma^{(l)}(\mathbf{x})] \right) \right], \quad (16)$$

where d_0 is the first layer input size. Clearly, the choice of $\sigma^{(l)}$ in each layer affects the total score.

Now consider a KAN network, where $\phi_{i,j}^{(l)}$ is the activation function that connects the i th input to the j th output in the l th layer. The total score $Q[\text{KAN}(\mathbf{x})]$ can be determined by treating each learned activation function separately and computing $Q[\phi_{i,j}^{(l)}(\mathbf{x})]$ using the method described in Section III-A. When computing the score for each activation function, we consider the derived symbolic expressions for $\phi_{i,j}^{(l)}$ and not the original B-spline implementation. Summing the individual scores across all activation functions in the KAN network, we obtain

$$Q[\text{KAN}(\mathbf{x})] = \sum_{l=1}^L \sum_{j=1}^{d_l} \sum_{i=1}^{d_{l-1}} \left(a_{i,j}^{(l)} \times Q[\phi_{i,j}^{(l)}(\mathbf{x})] \right). \quad (17)$$

Here, $a_{i,j}^{(l)}$ is 0 if $\phi_{i,j}^{(l)}$ is pruned and 1 otherwise. The pruning process is described in Section III-D1. We note that for KANs, the score of each $\phi_{i,j}^{(l)}$ is determined on the grid interval of the activation function. For MLPs, this interval can be chosen based on the domain, range, and boundedness of the activation function in each hidden layer.

D. Details for Further Improvements

1) **Pruning:** To further improve the energy efficiency of KANs, we utilize the pruning methodology in [5]. For a KAN with multiple layers, each neuron's importance is determined by incoming and outgoing scores

$$I_i^{(l)} = \max_k \left(\|\phi_{i,k}^{(l-1)}(x)\|_1 \right), \quad O_i^{(l)} = \max_j \left(\|\phi_{j,i}^{(l+1)}(x)\|_1 \right), \quad (18)$$

where $\phi_{i,k}^{(l-1)}(x)$ and $\phi_{j,i}^{(l+1)}(x)$ represent activation functions on edges to and from the i th neuron in the l th layer. Neurons with both scores above a threshold η are retained, and all others are pruned. For KAN layers, we can also consider pruning individual activation functions rather than neurons. In this case, $\|\phi_{i,k}^{(l-1)}(x)\|_1$ is considered for all activation functions, and the edge is pruned if this value is below η . Pruning will help obtain compact closed-form expressions by removing redundant activation functions, thereby improving energy efficiency.

2) **Training:** To optimize BLER performance, we employ noise-scheduling, and utilize the modified cross-

Algorithm 2 AE training with noise scheduling

Input: $m, B, \alpha, \sigma_{\max}^2, \sigma_{\min}^2, n_{\text{epochs}}$
Output: Optimized parameters $\{\theta_e, \theta_d\}$
 $\sigma_n^2 = \sigma_{\max}^2$
for $n = 1$ to n_{epochs} do
 Sample $\{m^{(i)}\}_{i=1}^B$ from m
 $s_{\text{tx}} = \text{Encoder}(m; \theta_e)$
 $s_{\text{rx}} = s_{\text{tx}} + w, w \sim \mathcal{CN}(0, \sigma^2)$
 $\hat{y} = \text{Decoder}(s_{\text{rx}}; \theta_d)$
 $\mathcal{L} \leftarrow (19)$
 Update θ_e and θ_d using \mathcal{L} and α
 $\sigma_n^2 = \sigma_{\max}^2 - (n/n_{\text{epochs}}) \times (\sigma_{\max}^2 - \sigma_{\min}^2)$
end

entropy loss function

$$\mathcal{L} = - \sum_{i=1}^{2^k} T_i \log \left(\frac{\exp(l_i)}{\sum_{j=1}^{2^k} \exp(l_j)} \right), \quad (19)$$

where T_i is the true label for the i th class, and l_i and l_j are the logarithmic odds for the i th and j th decoder output. The model outputs logarithmic odds directly, as there is no softmax layer at the decoder output. In this study, we use the Adam optimizer to adjust the encoder parameters θ_e and decoder parameters θ_d for joint training of the encoder and decoder. Algorithm 2 outlines this process, where B is the batch size, σ_{\min}^2 and σ_{\max}^2 give the noise scheduling range, and α is the learning rate.

IV. Numerical Results

For numerical experiments, we analyze (24,12) AEs in an end-to-end OFDM system as a proof-of-concept, with plans to use larger block size in future work. For comparison, we consider MLPs with a single input, hidden, and output layer. The hidden layer uses rectified linear unit (ReLU) activation functions, while the output layer has no activations. In this study, we consider MLPs with 150 hidden layer neurons at both the encoder and decoder. For the KAN-AE, we replace the MLPs with a single KAN layer at both the encoder and decoder, where each learnable activation function has 5 learnable control points c and uses third-degree polynomial basis functions. To avoid removing key components of the KAN-AE, we use a modest pruning threshold $\eta = 10^{-4}$ at the encoder and $\eta = 3 \times 10^{-5}$ at the decoder. During the SR procedure, we consider an error tolerance $\epsilon = 10^{-2}$ for the non-linearity score calculation described in Section III-A, and $\lambda = 3 \times 10^{-2}$ for the non-linearity score weight given in Section III-B.

We create, train, and test the MLP-AE and KAN-AE in Python using the PyTorch machine learning library. Adam is used to train each model in AWGN for 3×10^4 epochs, where each batch contains 2^{11} randomly selected m , and the learning rate is set to $\alpha = 10^{-3}$. We use $E_b/N_0 = 0$

dB to compute σ_{\min}^2 and $E_b/N_0 = 6$ dB to compute σ_{\max}^2 . The grid interval for each KAN activation function is updated periodically to fit the training examples. All models are trained using an NVIDIA RTX 3070 GPU. We compare the MLP-AE and KAN-AE to (24,12) Golay code with maximum-likelihood decoding (MLD). Our implementation of MLD for Golay code uses quadrature phase shift keying (QPSK) as the modulation scheme, where $\mathbb{E}[|s_{\text{tx}}|^2] = 1$. Let $\mathbf{s}_g \in \mathbb{C}^{n/2}$ be a vector of symbols forming a modulated codeword. We implement the MLD as

$$\hat{\mathbf{c}} = \arg \max_{\mathbf{c}} \text{Re}\{\mathbf{s}_g^H \mathbf{c}\}, \quad (20)$$

where $\hat{\mathbf{c}}$ is the detected modulated codeword and $\mathbf{c} \in \mathbb{C}^{n/2}$ is a vector containing a QPSK modulated codeword for the Golay code. For this implementation of MLD, the number of linear operations is $n^2 \times 2^k$, which we use to compute a non-linearity score of 2.359296×10^6 for (24,12) Golay MLD.

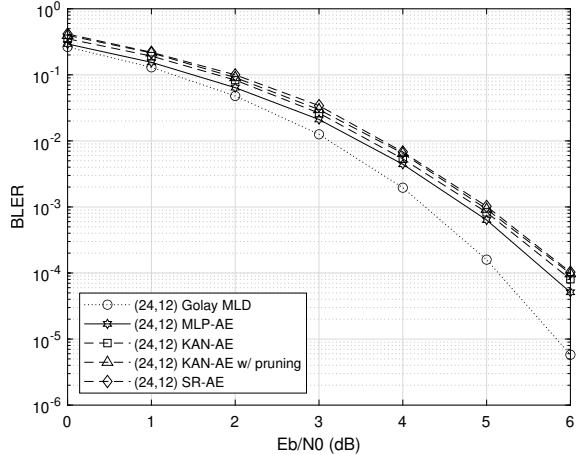
A. Block Error Rate Performance

To characterize the BLER performance, we perform Monte-Carlo experiments. First, we simulate the BLER in AWGN for the MLP-AE and KAN-AE, and compare it to (24,12) Golay MLD. The BLER curves in Fig. 2a show that the KAN-AE performs similarly to the MLP-AE and (24,12) Golay MLD, with (24,12) Golay MLD slightly outperforming both. Observe that the KAN-AE and MLP-AE perform almost identically. Additionally, in Fig. 2a, we see that pruning has a relatively minor effect on the overall BLER performance for the KAN-AE. We also note that the KAN-based symbolic regression autoencoder (SR-AE) showed no loss in performance compared to the pruned model.

We perform another Monte-Carlo experiment under a Rayleigh fading channel and again compare the BLER of the MLP-AE and KAN-AE to (24,12) Golay MLD. In this experiment, the symbols on each subcarrier observe flat-fading due to the use of OFDM, and we assume perfect channel estimation at the receiver. From Fig. 2b, we can see that all models show comparable performance. Additionally, similar to the AWGN channel, pruning has a slight negative effect on BLER performance, with the SR-AE showing nearly identical performance to the pruned model. The simulation results show that the SR-AE performs very similar to the original KAN-AE, thereby indicating that the model accuracy has been maintained.

B. Power and Energy Consumption

Another experiment is conducted where 5×10^3 messages m are processed using the MLP-AE, SR-AE, and Golay code, for a fixed 2.5×10^4 trials. We note that this simulation includes the encoder, channel, and decoder. We monitor the GPU power consumption during inference



(a) Block error rate in AWGN.

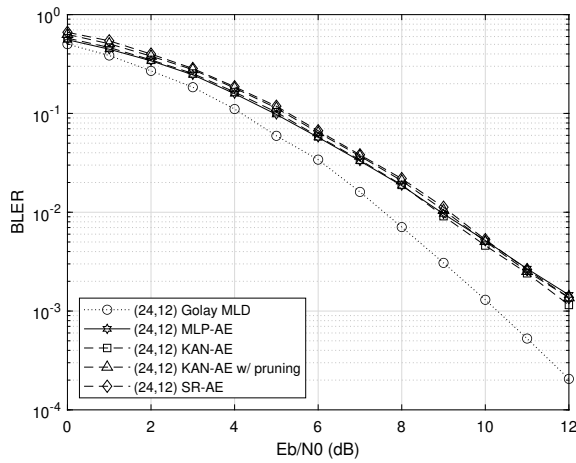


Fig. 2. Performance of different (24,12) coding schemes.

and compute the energy consumption for each model as the area underneath the power consumption curve. A comparison of the GPU power consumption over time for each scheme can be seen in Fig. 3. Since an NVIDIA RTX 3070 GPU is used in this experiment, the average power draw is very large in all cases; however, in a practical system like a radio or mobile device, the power draw can be significantly reduced at the cost of evaluation speed. Also, we emphasize that the curves seen in Fig. 3 are implementation and hardware dependent. Therefore, it is more appropriate to use the non-linearity score to access relative energy efficiencies of each scheme since it abstracts out the implementation and hardware details. In Fig. 3, we observe that the MLP-AE uses approximately 1.38 times more energy as compared to the KAN-based SR-AE. Here, we note that MLD for Golay code performs the best with respect to energy consumption, which can be explained by the hardware level optimizations of the PyTorch library by which it is implemented.

The peak power consumption, total energy consump-

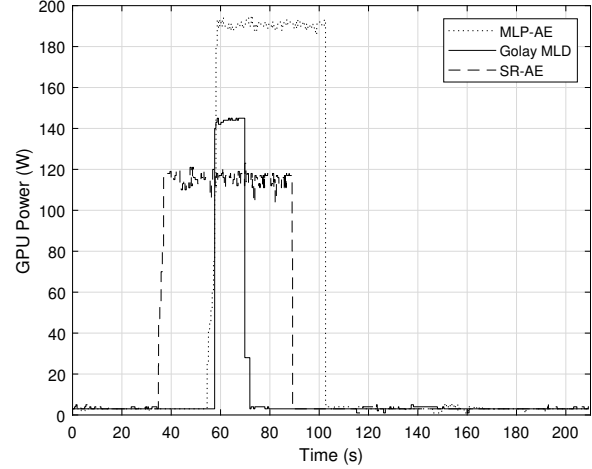


Fig. 3. GPU power consumption of (24,12) coding schemes during operation. Since this is a heuristic measurement, the non-linearity score offers a better, hardware and implementation-independent measure of the energy efficiency.

TABLE I
MLP-AE vs. SR-AE vs. Golay MLD

	MLP-AE	SR-AE	Golay with MLD
Peak power	195 W	123 W	145 W
Energy consumption	9166.9 J	6644.4 J	2420.0 J
Non-linearity score	1.2366e+6	6.8464e+5	2.3592e+6

tion, and non-linearity score for the MLP-AE and SR-AE are reported in Table I. To compute the non-linearity score for the MLP-AE, we consider the individual score for each ReLU activation function. Since ReLU is a piecewise linear function with $N = 2$, a score of 2 is assigned to each hidden layer activation. The output layer for both MLPs in the AE have no activation, so each output layer activation function is assigned a score of 0. Then, using (16), we calculate the score seen in Table I. Next, consider the KAN-AE, which is pruned and converted to symbolic expressions. Each activation function is considered on its grid interval, which is $[0, 1]$ for those in the encoder and $[-2.2, 2.2]$ for those in the decoder. Using (17), we calculate the score for the SR-AE seen in Table I.

V. Concluding Remarks

This study demonstrates that KANs can provide advantages over MLPs in terms of energy efficiency and model size for channel coding tasks. The ability to derive symbolic expressions from KANs allows for simplified, low-complexity equations, which reduces the computational burden during inference. To obtain simpler symbolic expressions, we propose a non-linearity metric, which we then use to score different symbolic expressions and eliminate unnecessary, highly non-linear activation functions during the SR process. Our results show that KAN-AEs perform similarly to MLP-AEs in AWGN and flat-fading Rayleigh channels, while achieving reduced energy con-

sumption when combined with the proposed SR method. This makes KANs a promising option for integrating DL models into energy-constrained devices within practical communication systems. Future work will focus on refining the non-linearity metric, considering larger codes, and performing a sensitivity analysis to examine how the score term impacts the SR process.

References

- [1] M. Soltani, V. Pourahmadi, A. Mirzaei, and H. Sheikhzadeh, “Deep learning-based channel estimation,” *IEEE Communications Letters*, vol. 23, no. 4, pp. 652–655, 2019.
- [2] M. Zhang, Y. Zeng, Z. Han, and Y. Gong, “Automatic modulation recognition using deep learning architectures,” in Proc. IEEE International Workshop on Signal Processing Advances in Wireless Communications (SPAWC), 2018, pp. 1–5.
- [3] Q. Mao, F. Hu, and Q. Hao, “Deep learning for intelligent wireless networks: A comprehensive survey,” *IEEE Communications Surveys & Tutorials*, vol. 20, no. 4, pp. 2595–2621, 2018.
- [4] H. Huang, S. Guo, G. Gui, Z. Yang, J. Zhang, H. Sari, and F. Adachi, “Deep learning for physical-layer 5G wireless techniques: Opportunities, challenges and solutions,” *IEEE Wireless Communications*, vol. 27, no. 1, pp. 214–222, 2020.
- [5] Z. Liu, Y. Wang, S. Vaidya, F. Ruehle, J. Halverson, M. Soljačić, T. Y. Hou, and M. Tegmark, “KAN: Kolmogorov-Arnold networks,” arXiv preprint arXiv:2404.19756, 2024.
- [6] R. Yu, W. Yu, and X. Wang, “KAN or MLP: A fairer comparison,” arXiv preprint arXiv:2407.16674, 2024.
- [7] Z. Liu, P. Ma, Y. Wang, W. Matusik, and M. Tegmark, “KAN 2.0: Kolmogorov-Arnold networks meet science,” 2024. [Online]. Available: <https://arxiv.org/abs/2408.10205>
- [8] C. J. Vaca-Rubio, L. Blanco, R. Pereira, and M. Caus, “Kolmogorov-Arnold networks (KANs) for time series analysis,” arXiv preprint arXiv:2405.08790, 2024.
- [9] T. O’Shea and J. Hoydis, “An introduction to deep learning for the physical layer,” *IEEE Transactions on Cognitive Communications and Networking*, vol. 3, no. 4, pp. 563–575, 2017.
- [10] A. Felix, S. Cammerer, S. Dörner, J. Hoydis, and S. Ten Brink, “OFDM-autoencoder for end-to-end learning of communications systems,” in Proc. IEEE International Workshop on Signal Processing Advances in Wireless Communications (SPAWC), 2018, pp. 1–5.
- [11] D. Wu, M. Nekovee, and Y. Wang, “Deep learning-based autoencoder for m-user wireless interference channel physical layer design,” *IEEE Access*, vol. 8, pp. 174 679–174 691, 2020.
- [12] A. K. Kolmogorov, “On the representation of continuous functions of several variables by superposition of continuous functions of one variable and addition,” *Doklady Akademii Nauk SSSR*, vol. 114, pp. 369–373, 1957.